

ARTICLE

Received 9 Jul 2012 | Accepted 14 Jan 2013 | Published 26 Feb 2013

DOI: 10.1038/ncomms2496

Enhanced dihydropyridine receptor calcium channel activity restores muscle strength in JP45/CASQ1 double knockout mice

Barbara Mosca¹, Osvaldo Delbono², Maria Laura Messi², Leda Bergamelli¹, Zhong-Min Wang², Mirko Vukcevic³, Ruben Lopez³, Susan Treves^{1,3}, Miyuki Nishi⁴, Hiroshi Takeshima⁴, Cecilia Paolini⁵, Marta Martini⁶, Giorgio Rispoli⁶, Feliciano Protasi⁵ & Francesco Zorzato^{1,3}

Muscle strength declines with age in part due to a decline of Ca^{2+} release from sarcoplasmic reticulum calcium stores. Skeletal muscle dihydropyridine receptors ($\text{Ca}_v1.1$) initiate muscle contraction by activating ryanodine receptors in the sarcoplasmic reticulum. $\text{Ca}_v1.1$ channel activity is enhanced by a retrograde stimulatory signal delivered by the ryanodine receptor. JP45 is a membrane protein interacting with $\text{Ca}_v1.1$ and the sarcoplasmic reticulum Ca^{2+} storage protein calsequestrin (CASQ1). Here we show that JP45 and CASQ1 strengthen skeletal muscle contraction by modulating $\text{Ca}_v1.1$ channel activity. Using muscle fibres from JP45 and CASQ1 double knockout mice, we demonstrate that Ca^{2+} transients evoked by tetanic stimulation are the result of massive Ca^{2+} influx due to enhanced $\text{Ca}_v1.1$ channel activity, which restores muscle strength in JP45/CASQ1 double knockout mice. We envision that JP45 and CASQ1 may be candidate targets for the development of new therapeutic strategies against decay of skeletal muscle strength caused by a decrease in sarcoplasmic reticulum Ca^{2+} content.

¹ Department of Experimental and Diagnostic Medicine, General Pathology section, University of Ferrara, Via Borsari 46, Ferrara 44121, Italy. ² Department of Physiology and Pharmacology, Wake Forest University School of Medicine, Winston-Salem, North Carolina 27157, USA. ³ Department of Biomedicine and Anesthesiology, Basel University Hospital, Hebelstrasse 20, Basel 4031, Switzerland. ⁴ Department of Biological Chemistry, Graduate School of Pharmaceutical Sciences, Kyoto University, Kyoto 606-8501, Japan. ⁵ CeSI-Center for Research on Ageing & DNI-Department of Neuroscience and Imaging, University Gabriele d'Annunzio of Chieti, Via Colle dell'Ara, 66100 Chieti, Italy. ⁶ Department of Biology and Evolution, Physiology and Biophysics University of Ferrara, Via Borsari 46, Ferrara 44121, Italy. Correspondence and requests for materials should be addressed to F.Z. (email: fzorzato@uhbs.ch).

Activation of skeletal muscle contraction is initiated by the propagation of the action potential deep into the muscle fibre by means of the transverse tubular system (T system)^{1–3}. T-tubule depolarization causes massive release of Ca^{2+} from the sarcoplasmic reticulum (SR) throughout the entire length of the muscle fibre by a process called excitation-contraction coupling^{1,2}. Loss of muscle function has been recognized as a debilitating and life-threatening condition not only in the elderly, but also in cachexia in cancer patients and in all those clinical conditions associated with prolonged bed rest^{4,5}. The decay of muscle strength is caused by several factors, including a decrease of releasable calcium from the skeletal muscle SR calcium store^{6,7}.

EC coupling is operated by a macromolecular complex comprising the α_1 -subunit of the voltage-dependent L-type Ca^{2+} channel (dihydropyridine receptor, DHPR, $\text{Ca}_v1.1$), the ryanodine receptor (RyR) and calsequestrin (CASQ1)⁸, in the contact region between the T system and the SR membrane³. $\text{Ca}_v1.1$ acts as a voltage sensor and generates orthograde signals that cause opening of the RyR whereby Ca^{2+} is released from the SR into the myoplasm, leading to activation of the contractile proteins¹. Analysis of voltage-dependent calcium currents in RyR1 knockout (KO) muscle cells was fundamental to clarify the signalling mechanisms between the RyR and $\text{Ca}_v1.1$. It is now accepted that the RyR1 not only receives an orthograde signal from $\text{Ca}_v1.1$, but also generates a retrograde signal which is important for the activation of $\text{Ca}_v1.1$ channel activity^{9,10}. The mechanism by which the retrograde Ca^{2+} current enhancement is modulated and its exact physiological role remain elusive.

Although calcium influx across the sarcolemma is thought to be non relevant for muscle contraction¹¹, it has been proposed that it may have a role in replenishing the SR during sustained muscle contractions¹². Two different modes of calcium influx in skeletal muscle have been described: (i) calcium influx via $\text{Ca}_v1.1$ associated with prolonged membrane depolarization is referred to as excitation-coupled calcium entry (ECCE)¹⁰, (ii) calcium influx via STIM1 and Ora1 stimulated by internal store depletion is referred to as store-operated calcium entry (SOCE)^{13–15}. However, the analysis of macroscopic calcium currents in adult muscle fibres recorded under voltage clamp condition¹⁶ suggests that both voltage-dependent calcium release and/or SR calcium depletion are not sufficient to activate inward calcium currents and thus challenged the physiological relevance of ECCE and SOCE in adult mammalian fibres. Nevertheless, calcium influx in muscle cells deserves further investigation, because of the potential impact of calcium influx in determining releasable SR calcium content¹⁷, a crucial factor for proper sustained muscle force development^{6,7,18}.

Calcium influx in skeletal muscle is affected by drugs^{19,20} and by accessory proteins such as junctophyllin and mitsugumin-29, two proteins localized in the membrane compartment which form the junction between T tubules and SR^{12,21}. T tubules-SR junction membranes encompasses also JP45, a developmentally regulated 45-kDa transmembrane protein that interacts *via* its luminal carboxy-terminal domain with CASQ1, the major calcium storage protein of SR, and with its amino terminal domain with $\text{Ca}_v1.1$ ²². Ablation of calsequestrin 1 in skeletal muscle fibres results in a decrease of total calcium

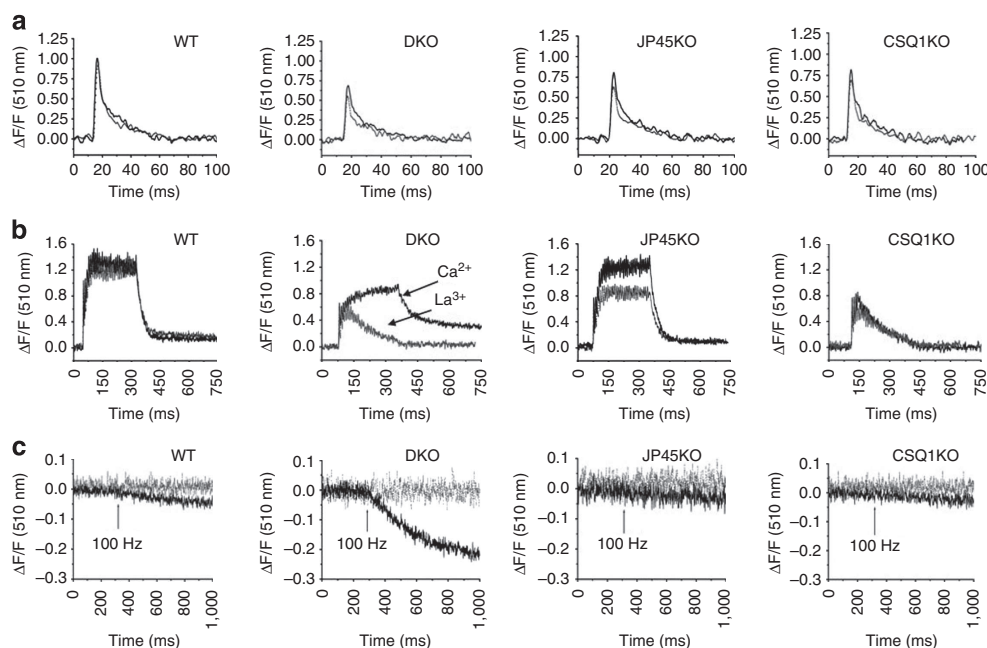


Figure 1 | Ca^{2+} transients and Mn^{2+} quenching in FDB fibres from single and DKO mice. FDB fibres were loaded with the fast low-affinity Ca^{2+} dye Mag-Fluo-4AM^{21,22}. **(a)** Ca^{2+} transients were triggered by supramaximal field stimulation with single pulses of 0.5 ms duration. Continuous lines: Ca^{2+} transients recordings in an external solution containing 1.8 mM CaCl_2 . Overall ANOVA P -value < 0.0001 ; multicomparison Dunnett's ANOVA post test shows difference between of the peak calcium values: WT versus DKO $P < 0.01$, WT versus JP45 KO $P < 0.01$; WT versus CASQ1 KO $P < 0.01$; dotted grey lines: Ca^{2+} transients recordings in an external solution containing 100 μM La^{3+} . Overall ANOVA P -value < 0.0001 ; multicomparison Dunnett's ANOVA post test shows difference between of the peak calcium values: WT versus DKO $P < 0.01$, WT versus JP45 KO $P < 0.01$, WT versus CASQ1 KO $P < 0.01$. **(b)** Recording of Ca^{2+} transients upon stimulation with repetitive pulses at 100 Hz for 300 ms duration. Black and grey lines show recordings in the presence of 1.8 mM Ca^{2+} and 100 μM La^{3+} in the external solution, respectively. In the presence of La^{3+} , the overall ANOVA P -value is < 0.0001 ; multicomparison Dunnett's ANOVA post test shows differences: WT versus DKO $P < 0.01$, WT versus JP45 KO $P < 0.05$, WT versus CASQ1 KO $P < 0.01$. **(c)** Mn^{2+} quenching of Fura-2 fluorescence. Black lines: Mn^{2+} influx was triggered by repetitive pulses at 100 Hz (arrow) for 300 ms duration. Overall ANOVA P -value < 0.0001 ; multicomparison Dunnett's ANOVA post test shows differences: WT versus DKO $P < 0.01$. Dotted grey lines: Mn^{2+} quenching recordings in the presence of 50 μM nifedipine in the external solution.

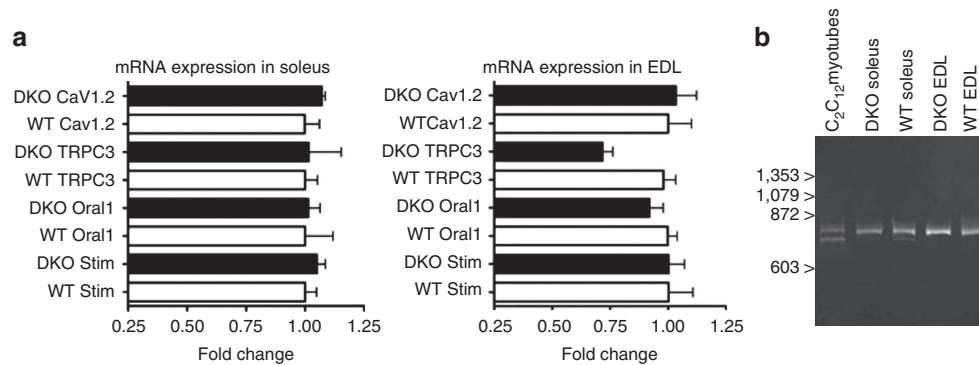


Figure 2 | Expression of calcium entry proteins in fast and slow muscles from DKO mice. (a) Real-time reverse transcription (RT) PCR from soleus and EDL of wild-type and DKO mice. Real-time RT PCR was carried out as previously described⁴¹. Briefly, total RNA was extracted using TRIzol reagent from Soleus or EDL muscles after frozen tissue homogenization, and Cav1.2, TRPC3, Oral1 and STIM1 gene expression was evaluated by quantitative real-time PCR. Boxes represent the mean (\pm s.e.m.) fold change compared with values obtained from WT for each gene of interest. Gene expression levels were normalized to the expression of the Tata box-binding protein (TBP) and desmin, whose expression was equal between wild-type and KO animals. Pooled data are results carried out on muscles from 5 to 7 different mice. (b) Expression of $\Delta 29$ Ca_v1.1 isoform mRNA in EDL and Soleus from 1-month-old WT and DKO mice. The expression of neonatal $\Delta 29$ Cav1.1 isoforms allele (lower band) is present in mRNA from C2C12 myotubes. The $\Delta 29$ Ca_v1.1 isoforms could be absent or below the detection limit of PCR in EDL. Soleus displays a faint band corresponding to the $\Delta 29$ exon Ca_v1.1 transcript.

release from the SR, which leads to impaired muscle performance and contractile activation^{23–26}. Chronic depletion of JP45 induces a decrease of muscle strength in 3-month-old JP45 KO mice²⁷. The decay in strength is apparently not linked to atrophy, but to defects in the EC-coupling machinery caused by alteration of the functional expression of DHPR Ca_v1.1 in the T-tubular network.

In the present study, we tested the hypothesis that the skeletal muscle Ca_v1.1 channel activity is not only regulated by the RyR, but additionally by the JP45/CASQ1 complex. We generated double JP45 and CASQ1 KO (DKO) and compared their Ca_v1.1-mediated Ca²⁺ signals to those observed in WT and each single JP45 and CASQ1 KO mice. Our results show that in DKO mice, tetanic stimulation of skeletal muscle fibres causes massive Ca²⁺ influx due to enhanced Ca_v1.1 channel activity and this Ca²⁺ influx restores muscle strength. By using this animal model, we have unveiled a signalling pathway which may be an important target for drugs against the loss of skeletal muscle strength caused by decrease of the SR calcium content.

Results

Calcium transient in flexor digitorum brevis fibres. We compared Ca²⁺ homeostasis in WT, single JP45 and CASQ1 KO and DKO using the ratiometric Ca²⁺ indicator Indo-1 and found that the resting calcium concentration was increased in DKO $1.15 \pm 0.23^*$ ($n=48$) fibres compared with WT (0.92 ± 0.10 , $n=40$), JP45 null (1.03 ± 0.18 , $n=42$) and CASQ1 null (0.95 ± 0.11) fibres (F_{405}/F_{480} indo-1 ratio values are mean \pm s.d.; *WT versus DKO $P<0.001$ two tailed Mann–Whitney). In the presence of 1.8 mM Ca²⁺ in the extracellular solution, the peak intracellular Ca²⁺ transients measured with the low-affinity calcium indicator MagFluo4 were 1.009 ± 0.18 ($n=47$), 0.67 ± 0.16 ($n=49$), 0.80 ± 0.25 ($n=40$) and 0.82 ± 0.25 ($n=47$) for WT, DKO, JP45 KO and CASQ1 KO, respectively ($\Delta F/F_0$ values are expressed as mean \pm s.d., Fig. 1 top panels). The significant decrease of the peak Ca²⁺ transient in DKO fibres is not due to a lower membrane density of RyRs (Supplementary Fig. S1). The half-time of the decay of the Ca²⁺ transients in flexor digitorum brevis (FDB) fibres from DKO mice was significantly slower compared with WT (3.7 ± 0.7 , $n=47$ and 4.8 ± 1.9 ms, $n=49$ in WT and DKO fibres, respectively. Analysis

of variance (ANOVA) P -values <0.0001 ; multicomparison Dunnett's post test WT versus DKO $P<0.01$).

Enhanced ECCE in FDB fibres from DKO mice. The slower decay of the calcium transients in FDB fibres from DKO mice is not due to a decrease of calcium uptake in to the SR by the Ca²⁺ pump because we did not observe a reduction of the SERCA1 and SERCA2 expression in DKO mice (Supplementary Fig. S1). The increase of the half-time of the decay of the calcium transient is rather linked to an influx of extracellular Ca²⁺, as in the presence of La³⁺, a non-specific calcium channel blocker¹⁰, the difference in the half-time for the decay of calcium transient between WT and DKO fibres disappears (3.1 ± 0.7 and 3.3 ± 1.1 ms for WT and DKO, respectively). The effect of La³⁺ was much more evident upon stimulation of FDB fibres with repetitive action potentials. In the presence of La³⁺, the Ca²⁺ transient amplitude of tetanic stimulation was highest in WT fibres (1.31 ± 0.28 ; $n=37$) compared with that of DKO ($0.62 \pm 0.14^*$, $n=34$), JP45 KO ($1.05 \pm 0.30^{\S}$, $n=26$) and CASQ1 ($0.70 \pm 0.15^*n=24$) ($\Delta F/F_0$ values are mean \pm s.d., * $P<0.01$, $^{\S}P<0.05$, (multicomparison Dunnett's ANOVA post test, Fig. 1). In CASQ1 null fibres, the summation of Ca²⁺ transient peaks was dramatically different compared with WT, JP45 null and DKO fibres. After the few initial peaks, which display an amplitude 50% lower compared with WT, the fused Ca²⁺ transients in CASQ1 KO fibres rapidly decayed to basal levels. This event reflects depletion of Ca²⁺ stores due to the ablation of the Ca²⁺ storage protein^{23–25}. However, at variance with CASQ1 null fibres, the double KO (DKO) fibres exhibit a sustained Ca²⁺ transient which persisted for the entire duration of the repetitive stimulation in the presence of calcium in the extracellular solution (Fig. 1 middle panels, arrow Ca²⁺).

Depolarization of DKO fibres causes massive Ca²⁺ influx. The sustained calcium transients evoked by tetanic stimulation in DKO fibres is caused by massive Ca²⁺ influx, as in the presence of 100 μ M La³⁺ in the external solution (Fig. 1 middle panel, arrow La³⁺), the Ca²⁺ transient curve overlapped with that of CASQ1 KO fibres. These data unambiguously demonstrate that ablation of JP45 in a CASQ1 null background unveils a robust Ca²⁺ influx component coupled to membrane depolarization.

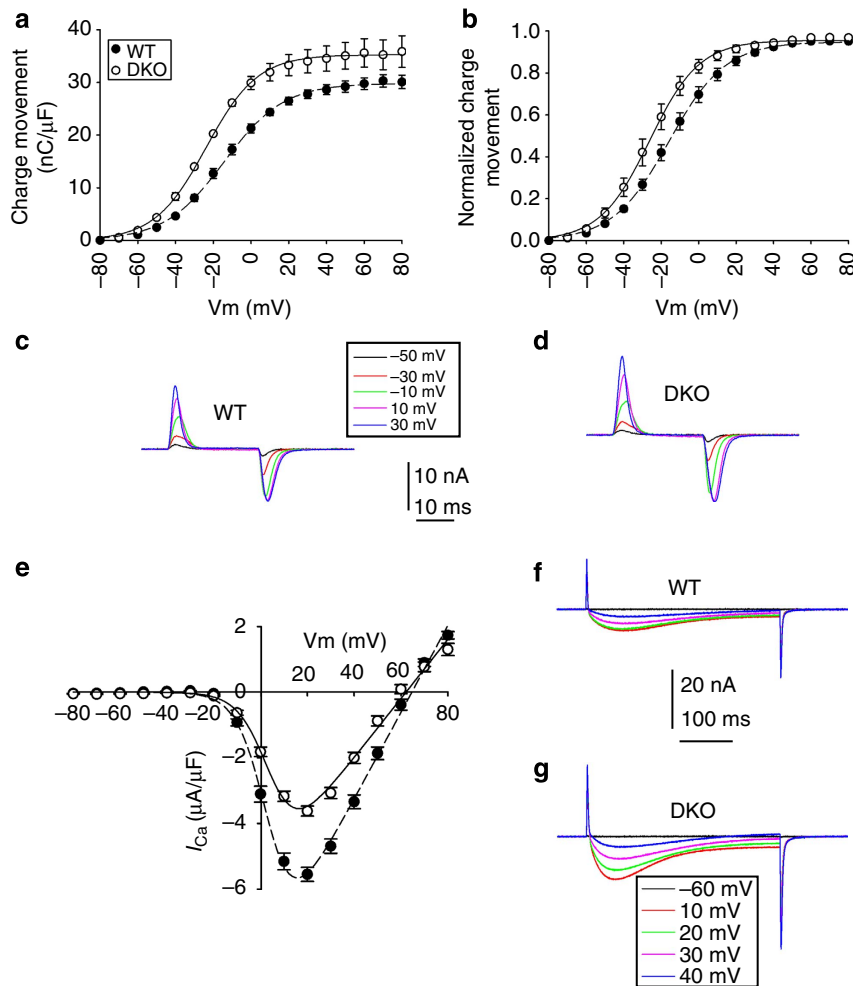


Figure 3 | Voltage dependence of charge movements and Ca^{2+} currents. (a) Charge movement–membrane potential relationship for WT ($n=13$) and DKO ($n=15$) muscle fibres. Values are mean \pm s.e.m. error bars show s.e.m. (b) Normalized values to maximal charge movement. Values are mean \pm s.e.m. error bars show s.e.m. (c–d) Representative charge movement traces recorded in FDB fibres voltage-clamped in the whole-cell configuration of the patch clamp. Holding potential: -80 mV. Command pulses of 25 ms duration evoked currents from -80 to 80 mV. Selected traces correspond to the steepest part of the curve. Notice the larger amplitude and 10 mV shift of the curve toward more negative potentials in DKO compared with WT mice. (e) Calcium current–membrane voltage relationship. Command pulses of 400 ms duration evoked currents from -80 to 80 mV. Notice the larger current amplitude for DKO ($n=19$) compared with WT ($n=29$) mice. Values are mean \pm s.e.m. (f–g) Representative calcium currents recorded at the indicated membrane voltages. Fitting curves, their respective equations and best fitting parameter values are described in Tables 1 and 2.

This conclusion is also supported by fura-2 manganese quenching experiments performed in FDB fibres (Fig. 1 lower panels). At an excitation wavelength of 360 nm, the Ca^{2+} independent isosbestic wavelength of fura-2, Mn^{2+} entry quenches fura-2 fluorescence²⁸. We measured the extent of the fluorescence quenching at the end of a 300-ms-long train of pulses at 100 Hz. We found that manganese quenching of fura-2 fluorescence was -0.11 ± 0.039 ($n=16$), -0.034 ± 0.021 ($n=17$), -0.034 ± 0.011 ($n=19$), -0.027 ± 0.019 ($n=35$) for DKO, WT, JP45 KO and CASQ1 KO fibres, respectively ($\Delta F/F_0$ values are mean \pm s.d.). The threefold increase of fura-2 fluorescence quenching by Mn^{2+} in DKO fibres was abolished by the addition of 50 μM nifedipine (Fig. 1 lower panels grey line), a specific inhibitor of $\text{Ca}_v1.1$ ¹⁰. Skeletal muscle membrane encompasses several molecules that can mediate calcium influx, including the neonatal splice variant ($\Delta 29$) of $\text{Ca}_v1.1$ ²⁹, TRPC3¹⁵ and Oral1/Stim1 ¹⁴, $\text{Ca}_v1.2$. We investigated the expression levels of other known calcium influx channels, and we found no changes both in fast and slow DKO fibres (Fig. 2). Altogether, these data support the conclusion that the increase of excitation-

coupled Mn^{2+} entry is mediated by an enhancement of calcium currents through adult form $\text{Ca}_v1.1$ ¹⁰. The next set of experiments was designed to evaluate the changes in the functional properties of the $\text{Ca}_v1.1$.

Increase of $\text{Cav}1.1$ channel activity in DKO fibres. The T-tubular system is the membrane compartment richest in $\text{Ca}_v1.1$ ³⁰ and high-resolution electron microscopy shows that volume and surface of the T-tubular system in FDB fibres from 1-month-old DKO and WT mice is not different (Supplementary Fig. S2). Thus, the threefold increase of excitation-coupled Mn^{2+} entry is not fully explained by changes of T-tubular membrane extensions or by a small increase of the $\text{Ca}_v1.1$ membrane density (Supplementary Fig. S1), but rather could be consistent with a modification of the channel activity of $\text{Ca}_v1.1$. To examine this possibility, we investigated the capacitive and Ca^{2+} currents of $\text{Ca}_v1.1$ in FDB fibres from DKO and WT mice by using the whole-cell configuration of the patch-clamp technique. Intact FDB fibres from DKO mice show 10 mV shift to more negative

Table 1 | Best-fitting parameters describing the voltage-dependence of charge movement.

	Q _{max} (nC μF ⁻¹)	V _{Q1/2} (mV)	K
WT (n = 13)	30 ± 8	-14 ± 2.2	16 ± 1.5
DKO (n = 15)	35 ± 11 (P = 0.724)	-24 ± 1.7 (P = 0.001)	14 ± 1.9 (P = 0.426)

Data points were fitted to a Boltzmann equation of the form: $Q_{on} = Q_{max} / [1 + \exp((V_{Q1/2} - V_m)/K)]$, where Q_{max} is the maximum charge, V_m is the membrane potential, $V_{Q1/2}$ is the charge movement half-activation potential and K is the steepness of the curve as described in ref. 27. The number of FDB fibres from three to four mice is between parentheses. Results are expressed as the mean ± s.e.m. Statistical significance was assessed using Student's *t*-test. The α -level was set at $P = 0.05$.

Table 2 | Best-fitting parameters describing the voltage-dependence of calcium current.

	G _{max} (nS/nF)	V _{1/2} (mV)	V _r (mV)	z
WT (n = 29)	90 ± 8	4.7 ± 2.5	62 ± 3.1	3.9 ± 0.6
DKO (n = 29)	132 ± 12 (P = 0.005)	3.8 ± 1.9 (P = 0.775)	64 ± 4.4 (P = 0.712)	4.0 ± 0.8 (P = 0.921)

Data points were fitted to the following equation: $I_{Ca} = G_{max} (V - V_m) / \{1 + \exp[zF(V_{1/2} - V)/RT]\}$, where G_{max} is the maximum conductance, V is the membrane potential, V_r is the reversal potential, $V_{1/2}$ is the half-activation potential, z is the effective valence, F is the Faraday constant, R is the gas constant and T is the absolute temperature (296 K) as described in ref. 43. The number of FDB fibres from three to four mice is between parentheses. Results are expressed as the mean ± s.e.m. Statistical significance was assessed using Student's *t*-test. The α -level was set at $P = 0.05$.

potential of the half maximal gating charge, and small nonsignificant increase (15%) in maximal gating charge, compared with control (Fig. 3b and Table 1). The small increase of maximal gating charges do not account for the ~45% increase of in peak Ca²⁺ current density, which was found in DKO FDB fibres (Fig. 3e). Half-maximal Ca²⁺ currents in wild-type (WT) and DKO mice were observed at very similar membrane potentials (Table 2). These results demonstrate that enhanced calcium influx is accounted for an increase of the Ca_v1.1 channel activity.

Skeletal muscle performance is restored in DKO mice. To investigate physiological relevance of the enhanced Ca_v1.1 channel activity in DKO mice, we measured *in vivo* muscle performance by assessing spontaneous motor activity (Fig. 4a). Three weeks of training improved skeletal muscle performance in both WT and KO mice, however, the total running distance in JP45 null and CASQ1 null mice was ~40 km lower compared with WT and DKO mice (139.7 ± 2.90 km, 118.1 ± 2.35 km versus 175.3 ± 2.96 km, 175.5 ± 4.23 km, respectively). The enhanced Cav1.1 channel activity restored muscle performance in DKO mice despite a low degree of atrophy of fast fibres (Supplementary Fig. S3), and may be a signature of improved muscle strength³¹ mediated by massive Ca²⁺ influx *via* Ca_v1.1¹⁰. To investigate this, we studied the mechanical properties of intact extensor digitorum longus (EDL) (Fig. 4b). EDL from WT and DKO were stimulated with a train of tetani at 0.27 Hz. The onset maximal tetanic force normalized per muscle cross-sectional area of EDL from WT and DKO were not significantly different (327.86 ± 117.53 mN versus 364.64 ± 76.22 mN, respectively; mean ± s.d. $n = 9$), whereas the time course of force development of EDL from DKO was dramatically different compared to those of WT. In DKO mice, the first train of repetitive pulses of 350 ms duration at 100 Hz caused an initial increase of isometric force and then rapidly decayed to ~20% of the onset value at the end of the repetitive pulses stimulation (Fig. 4b, arrow middle panel 'first'). The reduction of force development during trains of action

potentials is most likely indicative of poor calcium buffering capacity of SR caused by the ablation of CASQ1, as a similar inability to sustain muscle contraction has been observed in muscles from CASQ1 KO mice²⁴ but not in the EDL muscles from JP45 KO mice²⁷, which have a normal CASQ1 expression level. Ablation of JP45 in a CASQ1 KO background has a remarkable effect on the peak tension after repetitive tetanic trains at 0.27 Hz. We observed that in the EDL from the DKO mice the isometric tension developed at the end of the last pulse of the train increased up to 300% of the initial value while a modest decrease was evident in WT mice (Fig. 4b arrow middle panel 'last'; lower panels). On the basis of the data reported in Figs. 1 and 3, we reasoned that the ablation of JP45 in the CASQ1 KO background supports a strong calcium influx component mediated by Ca_v1.1 channel activity which leads to (i) accumulation of intracellular calcium and to (ii) the improvement of the peak force development after trains of tetanic stimulation. We tested this possibility by examining the effect of La³⁺ on the dynamics of force development of EDL from DKO mice during trains of tetani. As expected incubation of EDL with an external solution containing 100 μM La³⁺ blocked calcium influx, and the increase of isometric force at the end of each train of pulses at 100 Hz in DKO and had no effect on WT muscles (Fig. 4b, lower panels). The effect of La³⁺ in muscles from DKO mice was reversed by re-exposing EDLs to a bathing solution containing 1.8 mM CaCl₂ (Fig. 5).

Discussion

Here we investigated the role of the JP45/CASQ1 complex on the modulation of Ca_v1.1 function by analysing the functional properties of skeletal muscle fibres from JP45/CASQ1 DKO mice. Our results show that in DKO mice, calcium transients induced by repetitive action potential are supported by massive calcium influx from the extracellular environment. The massive increase of calcium influx is consistent with an enhancement of the Ca_v1.1 channel activity because: (1) it is inhibited by nifedipine, a blocker of Ca_v1.1; (2) it does not correlate with an increase in the expression of other known calcium influx channels such as Ora1, TRPC3 and the neonatal isoform of Ca_v1.1; (3) is associated with a 45% increase of the Ca_v1.1 peak calcium current density in intact single FDB fibres. This massive calcium influx *via* Ca_v1.1 restores the development of *in vitro* muscle force of EDL from DKO mice. The maintenance of muscle force *in vitro* is paralleled by the recovery of muscle performance of DKO mice *in vivo*. The characterization of the JP45/CASQ1 DKO animal model supports the conclusion that JP45/CASQ1 complex may be a genetically encoded modulator of the Ca_v1.1 channel activity.

The Ca_v1.1 complex has a dual function: it acts as (i) voltage sensor which activates, *via* a mechanical coupling, the RyR, and as (ii) a slow activating voltage-dependent calcium channel. Calcium influx *via* Ca_v1.1 channel activity was considered not important for skeletal muscle EC coupling, as it was shown that skeletal muscles can contract for hours in extracellular medium containing very low (sub nM) calcium concentrations¹¹. The idea that skeletal muscle EC coupling is independent from the influx of extracellular calcium was confirmed later by pharmacological and genetic manipulation of Ca_v1.1 function^{32–35}. However, in evaluating the functional significance of the Ca_v1.1 channel activity, one can not dismiss results showing that the influx of extracellular calcium is involved in the development of muscle contraction in amphibian and mammalian muscle fibres^{36,37}. This apparent discrepancy might be ascribed to different experimental models and conditions that were used to probe the importance of Ca_v1.1 channel activity in EC coupling. In this study we exploited the JP45/CASQ1 DKO mouse model to

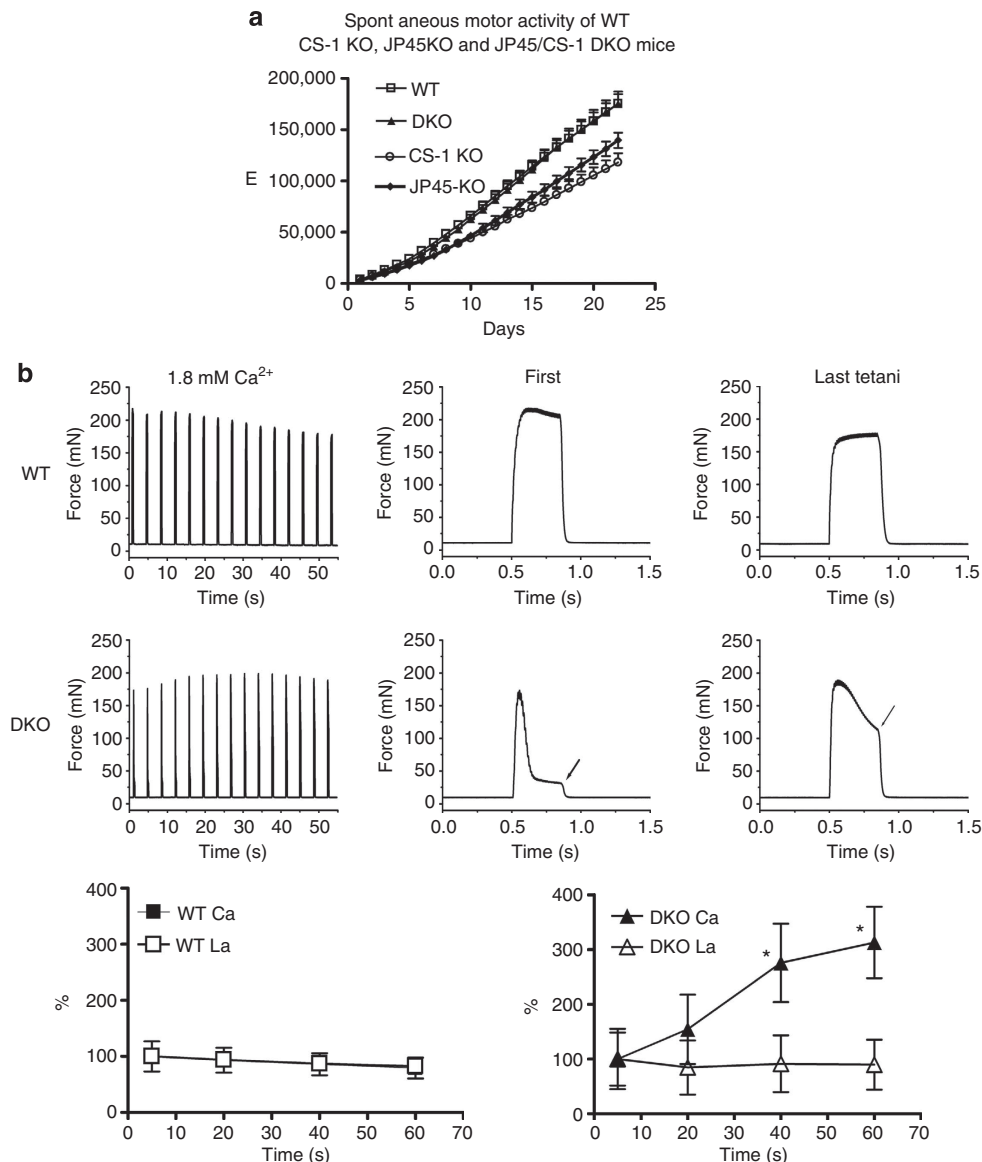


Figure 4 | Skeletal muscle performance of WT and DKO mice. (a) *In vivo* evaluation of muscle strength. Spontaneous activity in 4–6 week-old WT, DKO, JP45 KO and CASQ1 KO mice individually housed in cages equipped with a running wheel. Data points are expressed as mean \pm s.e.m.; $n = 10$ to 13 mice. Overall ANOVA P -value < 0.0001 ; multicomparison Dunnett's ANOVA post test shows difference: WT versus DKO $P > 0.05$; WT versus JP45 KO $P < 0.05$; WT versus CASQ1 KO $P < 0.01$. (b) Evaluation of tetanic force of intact EDL. Top and middle row of panels: EDLs were triggered by field stimulation in bathing solution containing 1.8 mM CaCl_2 with a train of repetitive pulses (100 Hz, 350 ms duration) at 0.27 Hz (left panels). Time course of force development of the first and last tetani of the trace displayed in the left panels (middle and right panels). Lower row of panels: after repetitive train stimulation the EDL muscles from control (left panel) and DKO (right panel) mice were incubated for 10 min in a bathing solution containing 100 μM La^{3+} and were then stimulated with repetitive trains of pulses at 0.27 Hz. Data point represents the force developed at the end of 350 ms duration repetitive pulse stimulation (values are mean \pm s.d. $n = 8$, * $P < 0.05$ Mann-Whitney). The increase the force developed at the end of tetanic stimulation in EDL from KO mice was abolished by 100 μM La^{3+} a blocker of the calcium influx into muscle fibres (compare DKO Ca^{2+} versus DKO La^{3+}).

investigate to role of $\text{Ca}_v1.1$ channel activity during EC coupling and its modulation by JP45/CASQ1 complex. Although we are aware that the JP45/CASQ1 KO mouse model may not recapitulate the physiological setting present in mammalian muscle fibres expressing normal levels of both JP45 and CASQ1, our data provide a strong case as to the potential physiological significance of the $\text{Ca}_v1.1$ channel activity during EC coupling, at least in mutant muscle fibres. The robust calcium influx via $\text{Ca}_v1.1$ channel activity which was observed during repetitive action potential in JP45/CASQ1 DKO mice results in better contractile function *in vitro* and, most importantly, *in vivo*. Such

an effect on muscle contractile function could reflect (i) an indirect global adaptive cellular response to the chronic ablation of two important SR proteins, or (ii) result from the lack of specific regulatory mechanism operated by the JP45/CASQ1 complex on the $\text{Ca}_v1.1$ channel activity. Although we cannot exclude any of the two possibilities, we are confident that our results clearly indicate the physiological importance of the dual activity of $\text{Ca}_v1.1$ during EC coupling of the DKO muscle fibres. In this mouse model $\text{Ca}_v1.1$ clearly operates not only as the voltage sensor that activates RyR (Fig. 2), (ii) but also as calcium influx channel which contribute to maintain an adequate level of

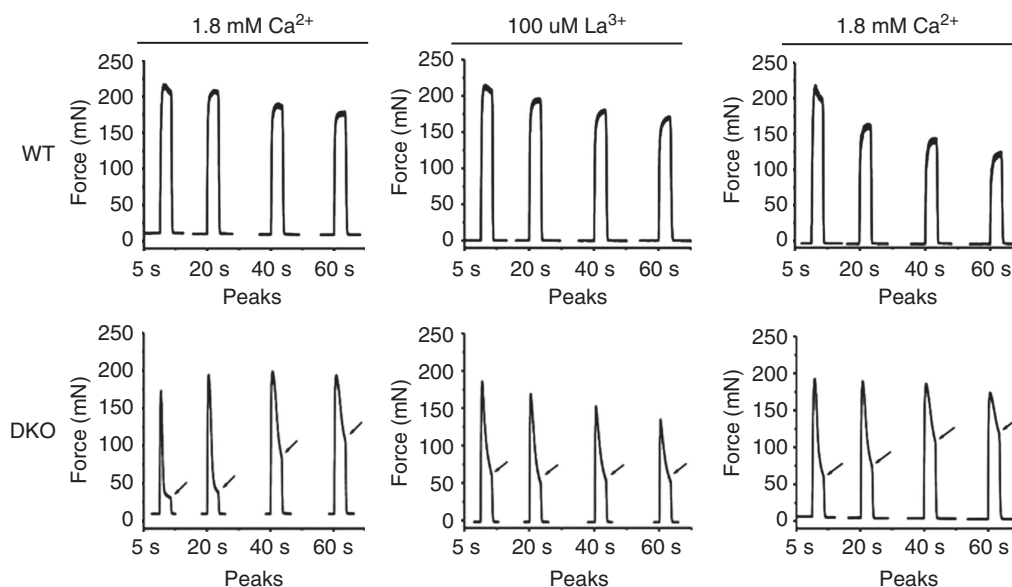


Figure 5 | Tetanic contraction of EDL from WT and JP45/CASQ1 double KO mice. EDL from wild-type and DKO were first incubated in a Tyrode's solution containing 1.8 mM CaCl₂. Maximal tetanic force was triggered by field stimulation with a train of repetitive pulses (100 Hz of 350 ms duration) at 0.27 Hz. Tetani at 5, 20, 40 and 60 s are shown. The same stimulation protocols was applied to muscle which were incubated for 10 min in a bathing solution containing 100 μM La³⁺ (traces WT La³⁺ and DKO La³⁺). The increase the force developed at the end of tetanic stimulation in EDL from KO mice was abolished by 100 μM La³⁺ a blocker of the calcium influx into muscle fibres (compare DKO left panel with middle panel). The effect of La³⁺ was reversed by 10 min long exposure of EDL muscles to a bathing solution containing Ca²⁺ (right panels).

releasable SR calcium content during sustained muscle activity evoked by tetanic stimulation (Fig. 3). These data imply that the JP45/CASQ1 complex modulate Ca_v1.1 channel activity also in normal fibres, in particular, it may operate in those conditions which causes a deficit SR calcium load.

On the basis of these data we propose that JP45/CASQ1 complex is genetically encoded modulator of the Ca_v1.1 channel activity, and that it constitutes a potential target to devise novel therapeutic strategies against the decline of skeletal muscle strength linked to decreased SR calcium content^{6,7,12}.

Methods

Generation JP45 CASQ1 DKO mice. JP45 KO was obtained as described by Delbono *et al.*²⁷. CASQ1 KO mice were obtained as described by Paolini *et al.*²⁶. DKO mice were generated by crossing to each other established JP45 KO and CASQ1 KO lines backcrossed in C57BL/6J (Supplementary Fig. S4).

Morphology. Immunohistochemistry of EDL and Soleus was carried out as described by Delbono *et al.*³⁸. EDL and soleus muscles were embedded in OCT, snap-frozen in isopentane, cryosectioned at the mid-belly region (10 μm) and mounted on coverslips for immunostaining. For staining mounted sections were air dried, treated with PBS containing 1% bovine serum albumin (BSA) and 2% horse serum for 30 min and incubated overnight at 4–8 °C with a PBS solution containing 0.01% Triton X100, 1% BSA, 2% horse serum, 0.5% μg ml⁻¹ anti-mouse slow myosin heavy chain (MAB 1628, Millipore, Billerica, MA), 2 μg ml⁻¹ anti rat α-laminin (MAB1914, Millipore). Sections were then washed with PBS for 15 min four times, and incubated at room temperature for 40 min with a PBS containing Alexa Fluor 488 anti-mouse IgG Ab (2 μg ml⁻¹) and Cy3 anti rat IgG Ab (0.5 μg ml⁻¹). After incubating in the secondary Ab, sections were washed with PBS for 15 min four times, dehydrated with ethanol and mounted using a glycerol medium. Fluorescence images were imaged using a Leica DM5000B fluorescence microscope and analysed with Analysis software package from Soft Imaging System, Muenster, Germany. Image analysis of muscle sections was performed in four steps: (1) determination of the muscle fibre boundaries, (2) determination of the muscle fibre cross-sectional area, (3) calculation of the per cent of muscle fibres positive for anti MHC I Ab and (4) determination of the per cent of muscle fibres negative for anti MHC I Ab staining. The muscle fibre cross-sectional area was determined using the minimal 'Ferret's diameter' (the minimum distance of parallel tangents at opposing borders of the muscle fibre). High-resolution electron microscopy was carried out as described by Paolini *et al.*²⁶ Volume and surface of the transverse tubule (TT)

network (see Table in Supplementary Fig. 4) were determined using the well-established stereology point and intersection counting techniques^{39,40} in EM micrographs taken at ×14,000 of magnification. (a) Measurement of relative fibre volume occupied by TT. After covering the images with an orthogonal array of dots at a spacing of 0.20 μm, the ratio between numbers of dots falling in the TT lumen and the total number of dots covering the whole image represent the relative volume of fibre occupied by the TT. (b) Measurement of TT surface area to volume. The images were covered with two sets of grid lines separated by a distance of 0.24 μm and intersecting at right angles. The frequency of intersections between the membrane of interest (TT profiles) and the grid lines was counted. The ratio of TT surface area to volume was obtained from the formula $C/2dP$ test, where C is the number of intersections, d is the spacing between the grid lines, and P test is the number of grid intersections in the test area.

Gene expression analysis. Expression of neonatal Δ29 isoform of Ca_v1.1 was detected by semiquantitative RT-PCR⁴¹. Total RNA was extracted from homogenized mouse muscle tissues EDL and SOL, and cultured C2C12 myotubes using TRIzol reagent. Eight hundred nanograms of RNA were first reverse transcribed into cDNA; the Cav1.1 cDNA was amplified by PCR using primers²⁹, which span exons 27–34: forward 5'-AGTCGGAGCAGATGAACCAC-3' and reverse 5'-ATGGCCTTGAACCTCATCCAG-3'. The PCR amplification conditions were 95 °C for 5 min, followed by 37 cycles of 94 °C for 40 s, 51 °C for 40 s and 70 °C for 1 min, followed by a 5-min extension at 72 °C. The RT-PCR products encoding the adult and neonatal (Ca_v1.1Δ29) isoforms are 790-bp long (upper band) and (lower band) 733 bp long, respectively.

Analysis of total SR and muscle strength assessment. Total SR membranes were prepared²² starting from a 20% skeletal muscle total homogenate; this was sedimented at 3,000_g for 10 min and the resulting supernatant was centrifuged at 15,000_g for 20 min to remove the myofibrillar protein components. The 15,000_g supernatant was then centrifuged for 60 min at 100,000_g to isolate the total SR (microsomal) pellet. SDS-polyacrylamide electrophoresis and western blot of total SR proteins were carried out as described by Anderson *et al.*²² Blots were probed with a polyclonal primary Ab followed by peroxidase-conjugated secondary antibodies. The immunopositive bands were visualized by chemiluminescence using the Super Signal West Dura kit from Thermo Scientific. Densitometry of the immunopositive bands was carried out by using BioRad GelDoc 2000. [³H]-PN200-110 and [³H]-Ryanodine binding was carried out according to Anderson *et al.*⁴² Briefly, total SR membranes were incubated for 1 h in the dark in a solution containing 50 mM Tris-HCl pH 7.5, 10 mM CaCl₂ plus protease inhibitor cocktail (ROCHE cat. no. 05892953001), 0.05–5 nM PN200-100 and (+)-[5-methyl-³H]. The samples were then filtered through Whatman glass microfibre GF/B filters by Millipore manifold filtering apparatus, rinsed three times

with 5 ml of solution containing 200 mM choline chloride, 20 mM Tris-HCl pH 7.5, and the radioactivity retained on the filters was determined by liquid scintillation counting. [³H]-ryanodine binding was carried out by incubating total SR membranes for 12–16 h at room temperature with 20 mM HEPES pH 7.4, 1 M NaCl, 5 mM AMP, 20 μM CaCl₂, 0.05–10 nM [³H]-ryanodine and protease inhibitor cocktail (ROCHE cat. no. 05892953001). Membrane bound [³H]-ryanodine was determined by scintillation counting as described above. Non-specific binding was evaluated in the presence of 1 μM unlabelled nifedipine and 10 μM unlabelled ryanodine, respectively. Curve fitting was performed using Graph Pad Prism 4 software package. Skeletal muscle performance and mechanical properties of EDL were analysed as described by Debono *et al.*²⁷ Briefly, animals were individually housed in cages equipped with a running wheel carrying a magnet. Wheel revolutions were registered by a reed sensor connected to an I-7053D Digital-Input module (Spectra AG, Egg, Switzerland), and the revolution counters were read by a standard laptop computer via an I-7520 RS-485-to-RS-232 interface converter (Spectra AG, Egg, Switzerland). Digitized signals were processed by the ‘mouse running’ software developed at Santhera Pharmaceuticals, Liestal, Switzerland. To test force *in vitro*, EDL muscles were dissected and mounted into a muscle testing set-up (Heidelberg-Scientific Instruments, Heidelberg, Germany). Muscle force was digitized at 4 kHz using an AD Instruments converter and stimulated with 15 V pulses for 0.5 ms. EDL tetanus was recorded in response to 400 ms pulses at 10–120 Hz. Specific force was normalized to the muscle cross-sectional area (CSA) = wet weight (mg)/length (mm) × 1.06 (density mg mm⁻³).

Cell electrophysiology recordings and optical recording. FDB fibres from WT and DKO mice were enzymatically dissociated, plated and recorded following published procedures^{43,44}. The composition of the pipette solution was (mM): 140 Cs-aspartate; 5 Mg-aspartate₂; 10 Cs₂EGTA (ethylene glycol-bis(α-aminoethyl ether)-N,N,N',N'-tetraacetic acid), 10 HEPES (N-[2-hydroxyethyl]piperazine-N'-[2-ethanesulfonic acid]), pH was adjusted to 7.4 with CsOH. The external solution contained (mM): 145 TEA (tetraethylammonium hydroxide)-Cl, 10 CaCl₂, 10 HEPES and 0.001 tetrodotoxin. Solution pH was adjusted to 7.4 with TEA.OH. For charge movement recording, calcium current was blocked with the addition of 0.5 Cd²⁺ plus 0.3 La³⁺ to the external solution⁴³. Peak Ca²⁺ currents were normalized to membrane capacitance and expressed as Amperes per Farad, whereas intramembrane charge movements were calculated as the integral of the current in response to depolarizing pulses and expressed per membrane capacitance as Coulombs per Farad. Fura-2 Mn²⁺ quenching in intact FDB fibres was carried out as previously described^{19,28}. Calcium transients were measured by using the low-affinity fluorescent calcium indicator MagFluo4^{45,46}. Briefly, changes in the [Ca²⁺]_i induced by supramaximal field stimulation were monitored in FDB fibres loaded with Mag-Fluo-4/AM in Tyrode's buffer. All experiments were carried out at room temperature (20–22 °C) in the presence of 50 μM N-benzyl-p-toluenesulfonamide (BTS) (Tocris) to minimize movement artefacts. Measurements were carried out with a Nikon ECLIPSE TE2000-U inverted fluorescent microscope equipped with a ×20 magnification objective. Fluorescent signals were captured by a photomultiplier connected to a Nikon Photometer P101 amplifier. Calcium transients were analysed by ADInstrument Chart5 and Origin.6 programs. Changes in fluorescence were calculated as ΔF/F = (F_{max} – Frest)/Frest. Resting calcium was measured with Indo1 loaded FDB fibres⁴⁵.

Statistical analysis. We used GraphPad Prims 4.0 software package to perform curve fitting and statistical analysis.

References

- Rios, E. & Pizarro, G. Voltage sensor of excitation-contraction coupling in skeletal muscle. *Physiol. Rev.* **71**, 849–908 (1991).
- Tanabe, T., Beam, K. G., Powell, J. A. & Numa, S. Restoration of excitation-contraction coupling and slow calcium current in dysgenic muscle by dihydropyridine receptor complementary DNA. *Nature* **336**, 134–139 (1990).
- Franzini-Armstrong, C. & Jorgensen, A. O. Structure and development of E-C coupling units in skeletal muscle. *Annu. Rev. Physiol.* **56**, 509–534 (1994).
- Manini, T. M. & Clark, B. C. Dynapenia and aging: an update. *J. Gerontol. A Biol. Sci. Med. Sci.* **67**, 28–40 (2012).
- Dodson, S. *et al.* Muscle wasting in cancer cachexia: clinical implications, diagnosis, and emerging treatment strategies. *Annu. Rev. Med.* **62**, 265–279 (2011).
- Kabbara, A. A. & Allen, D. G. The role of calcium stores in fatigue of isolated single muscle fibres from the cane toad. *J. Physiol.* **519**, 169–176 (1999).
- Andersson, D. C. *et al.* Ryanodine receptor oxidation causes intracellular calcium leak and muscle weakness in aging. *Cell Metab.* **14**, 196–207 (2011).
- Treves, S. *et al.* Minor sarcoplasmic reticulum membrane components that modulate excitation-contraction coupling in striated muscles. *J. Physiol.* **587**, 3071–3079 (2009).
- Nakai, J. *et al.* Enhanced dihydropyridine receptor channel activity in the presence of ryanodine receptor. *Nature* **380**, 72–75 (1996).
- Bannister, R. A., Pessah, I. N. & Beam, K. G. The skeletal L-type Ca²⁺ current is a major contributor to excitation-coupled Ca²⁺ entry. *J. Gen. Physiol.* **133**, 79–91 (2008).
- Armstrong, C. M., Bezanilla, F. M. & Horowicz, P. Twitches in the presence of ethylene glycol bis(α-aminoethyl ether)-N,N'-tetracetic acid. *Biochim. Biophys. Acta.* **267**, 605–608 (1972).
- Pan, Z. *et al.* Dysfunction of store-operated calcium channel in muscle cells lacking mg29. *Nat. Cell Biol.* **4**, 379–383 (2002).
- Kurebayashi, N. & Ogawa, Y. Depletion of Ca²⁺ in the sarcoplasmic reticulum stimulates Ca²⁺ entry into mouse skeletal muscle fibres. *J. Physiol.* **533**, 185–199 (2001).
- Yarotsky, V. & Dirksen, R. T. Temperature and RyR1 regulate the activation rate of store-operated Ca²⁺ entry current in myotubes. *Biophys. J.* **103**, 202–211 (2012).
- Launikonis, S. & Rios, S. Store-operated Ca²⁺ entry during intracellular Ca²⁺ release in mammalian skeletal muscle. *J. Physiol.* **583**, 81–97 (2007).
- Allard, B., Couchoux, H., Pouvreau, S. & Jacquemond, V. Sarcoplasmic reticulum Ca²⁺ release and depletion fail to affect sarcolemmal ion channel activity in mouse skeletal muscle. *J. Physiol.* **575**, 69–81 (2006).
- Rios, E. The cell boundary theorem: a simple law of the control of cytosolic calcium concentration. *J. Physiol. Sci.* **60**, 81–84 (2010).
- Allen, D. G., Lamb, G. D. & Westerblad, H. Impaired calcium release during fatigue. *J. Appl. Physiol.* **104**, 296–330 (2008).
- Cherednichenko, G. *et al.* Enhanced excitation-coupled calcium entry in myotubes expressing malignant hyperthermia mutation R163C is attenuated by dantrolene. *Mol. Pharmacol.* **73**, 1203–1212 (2008).
- Zhao, X. *et al.* Azumolene inhibits a component of store-operated calcium entry coupled to the skeletal muscle ryanodine receptor. *J. Biol. Chem.* **281**, 33477–33486 (2006).
- Hirata, Y. *et al.* Uncoupling store-operated Ca²⁺ entry and altered Ca²⁺ release from sarcoplasmic reticulum through silencing of junctophilin genes. *Biophys. J.* **90**, 4418–4427 (2006).
- Anderson, A. A. *et al.* The junctional SR protein JP-45 affects the functional expression of the voltage-dependent Ca²⁺ channel Cav1.1. *J. Cell Sci.* **19**, 2145–2155 (2006).
- Canato, M. *et al.* Massive alterations of sarcoplasmic reticulum free calcium in skeletal muscle fibers lacking calsequestrin revealed by a genetically encoded probe. *Proc. Natl Acad. Sci. USA* **107**, 22326–22331 (2010).
- Olojo, R. O. *et al.* Mice null for calsequestrin 1 exhibit deficits in functional performance and sarcoplasmic reticulum calcium handling. *PLoS One* **6**, e27036 (2012).
- Sztretzy, M. *et al.* Measurement of RyR permeability reveals a role of calsequestrin in termination of SR Ca(2+) release in skeletal muscle. *J. Gen. Physiol.* **138**, 231–247 (2011).
- Paolini, C. *et al.* Reorganized stores and impaired calcium handling in skeletal muscle of mice lacking calsequestrin-1. *J. Physiol.* **583**, 767–784 (2007).
- Delbono, O. *et al.* Loss of skeletal muscle strength by ablation of the sarcoplasmic reticulum protein JP45. *Proc. Natl Acad. Sci. USA* **104**, 20108–20113 (2007).
- Clementi, E. *et al.* Receptor-activated Ca²⁺ influx. Two independently regulated mechanisms of influx stimulation coexist in neurosecretory PC12 cells. *J. Biol. Chem.* **267**, 2164–2172 (1992).
- Tuluc, P. *et al.* A Cav1.1 Ca²⁺ channel splice variant with high conductance and voltage-sensitivity alters EC coupling in developing skeletal muscle. *Biophys. J.* **96**, 35–44 (2009).
- Fosset, M., Jaimovich, E., Delpont, E. & Lazdunski, M. [³H]nitrendipine receptors in skeletal muscle. *J. Biol. Chem.* **258**, 6086–6092 (1983).
- Brooks, S. V. & Faulkner, J. A. Skeletal muscle weakness in old age: underlying mechanisms. *Med. Sci. Sports Exerc.* **26**, 432–439 (1994).
- Gonzales-Serratos, H., Valle-Aguilera, R., Lathrop, D. A. & Garcia, M. C. Slow inward calcium currents have no obvious role in muscle excitation-contraction coupling. *Nature* **298**, 292–41982 (1982).
- Miledi, R., Parker, I. & Zhu, P. H. Extracellular ions and excitation-contraction coupling in frog twitch muscle fibres. *J. Physiol.* **351**, 687–710 (1984).
- Melzer, W., Herrmann-Frank, A. & Lüttgau, H. C. The role of Ca²⁺ ions in excitation-contraction coupling of skeletal muscle fibres. *Biochim. Biophys. Acta.* **1241**, 59–116 (1995).
- Dirksen, R. T. & Beam, K. G. Role of calcium permeation in dihydropyridine receptor function. Insights into channel gating and excitation-contraction coupling. *J. Gen. Physiol.* **114**, 393–403 (1999).
- Ildefonse, M., Jacquemond, V., Rougier, O., Renaud, J. F., Fosset, M. & Lazdunski, M. Excitation contraction coupling in skeletal muscle: evidence for a role of slow Ca²⁺ channels using Ca²⁺ channel activators and inhibitors in the dihydropyridine series. *Biochem. Biophys. Res. Commun.* **129**, 904–909 (1985).
- Lamb, G. D. Asymmetric charge movement in contracting muscle fibres in the rabbit. *J. Physiol.* **376**, 63–83 (1986).

38. Delbono, O. *et al.* Endogenously determined restriction of food intake overcomes excitation-contraction uncoupling in JP45KO mice with aging. *Exp. Gerontol.* **47**, 304–316 (2012).
39. Loud, A. V., Barany, W. C. & Pack, B. A. Quantitative Evaluation of Cytoplasmic Structures in Electron Micrographs. *Lab. Invest.* **14**, 996–1008 (1965).
40. Mobley, B. A. & Eisenberg, B. R. Sizes of components in frog skeletal muscle measured by methods of stereology. *J. Gen. Physiol.* **66**, 31–45 (1975).
41. Vukcevic, M., Spagnoli, G. C., Iezzi, G., Zorzato, F. & Treves, S. Ryanodine receptor activation by Ca^v1.2 is involved in dendritic cell major histocompatibility complex class II surface expression. *J. Biol. Chem.* **283**, 34913–34922 (2008).
42. Anderson, K., Cohn, A. H. & Meissner, G. High-affinity [³H]PN200-110 and [³H]ryanodine binding to rabbit and frog skeletal muscle. *Am. J. Physiol.* **266**, C462–C466 (1994).
43. Wang, Z. M., Messi, M. L. & Delbono, O. Patch-clamp recording of charge movement, Ca²⁺ current and Ca²⁺ transients in adult skeletal muscle fibers. *Biophys. J.* **77**, 2709–2716 (1999).
44. Hernández-Ochoa, E. O. & Schneider, M. F. Voltage clamp methods for the study of membrane currents and SR Ca²⁺ release in adult skeletal muscle fibres. *Prog. Biophys. Mol. Biol.* **108**, 98–118 (2012).
45. Hollingworth, S., Gee, K. R. & Baylor, S. M. Low-affinity Ca²⁺ indicators compared in measurements of skeletal muscle Ca²⁺ transients. *Biophys. J.* **97**, 1864–1872 (2009).
46. Calderón, J. C., Bolaños, P. & Caputo, C. Myosin heavy chain isoform composition and Ca²⁺ transients in fibres from enzymatically dissociated murine soleus and extensor digitorum longus muscles. *J. Physiol.* **588**, 267–279 (2010).
47. Tomasi, M. *et al.* Calsequestrin (CASQ1) rescues function and structure of calcium release units in skeletal muscles of CASQ1-null mice. *Am. J. Physiol. Cell Physiol.* **302**, C575–C586 (2012).

Acknowledgements

This work was supported by funds from Swiss Muscle foundation, A.F.M., S.N.F and Department of Biomedicine University Hospital Basel. This study was also supported by Research Grant no. GGP08153 from the Italian Telethon ONLUS Foundation to F.P. and grants from the NIH/NIA (AG13934 and AG15820) to O.D.

Author contributions

B.M. and L.B. developed and monitored mouse colony, collected and analysed calcium measurements data; M.V. collected and analysed expression data; R.L. collected and analysed force measurements data; M.T. and H.T. generated mice model; C.P. and F.P. provided CASQ1 KO mice and performed structural analysis; O.D., M.L.M., Z.-M.W., M.M. and G.R. collected and analysed electrophysiological data; S.T. collected and analysed biochemical data; and F.Z. took care of conception and design of the experiments, collection and analysis of biochemical, histochemistry and physiological data, and drafting of the manuscript.

Additional information

Supplementary Information accompanies this paper at <http://www.nature.com/naturecommunications>

Competing financial interests: The authors declare no competing financial interests.

Reprints and permission information is available online at <http://npg.nature.com/reprintsandpermissions/>

How to cite this article: Mosca, B. *et al.* Enhanced dihydropyridine receptor calcium channel activity restores muscle strength in JP45/CASQ1 double knockout mice. *Nat. Commun.* **4**:1541 doi: 10.1038/ncomms2496 (2013).